IEEE Access
Multidisciplinary ⋮ Rapid Review ⋮ Open Access Journal

Received February 16, 2021, accepted February 28, 2021, date of publication March 10, 2021, date of current version March 22, 2021.

Digital Object Identifier 10.1109/ACCESS.2021.3065269

Adaptive Background Compensation of Frequency Interleaved DACs With Application to Coherent Optical Transceivers

AGUSTÍN C. GALETTO[1], (Graduate Student Member, IEEE), BENJAMÍN T. REYES[1], DAMIÁN A. MORERO[2], AND MARIO R. HUEDA[2,3]

[1]Fundación Fulgor, Córdoba 5000, Argentina
[2]Laboratorio de Comunicaciones Digitales, Universidad Nacional de Córdoba, Córdoba 5000, Argentina
[3]National Scientific and Technological Research Council of Argentina (CONICET), Córdoba 5000, Argentina

Corresponding author: Agustín C. Galetto (agaletto@fundacionfulgor.org.ar)

This work was supported by Fundación Fulgor.

ABSTRACT Digital-to-analog converters (DACs) with bandwidths larger than 70 GHz and sampling rates in excess of 170 GS/s will soon be required in ultra-high speed communication applications such as coherent optical transceivers operating at symbol rates of 140 GBd and beyond. Frequency interleaving has been proposed as a way to break the bandwidth bottleneck in such applications. Splitting the input signal into multiple frequency bands reduces the required bandwidth per interleaved DAC and therefore it enables the synthesis of greater bandwidth signals in the reconstructed output. Elaborate digital signal processing (DSP) is required to seamlessly stitch together the sub-bands and compensate the errors of the analog signal path, which would otherwise severely degrade the performance of the communication system. Adaptive DSP techniques are required to automatically compensate errors caused by process, voltage, and temperature variations in the technology (e.g., CMOS, SiGe, etc.) implementations of the data converters, and therefore ensure high manufacturing yield. These techniques must operate in background mode to avoid interfering with the normal operation of the communication system. This work introduces an adaptive background compensation scheme for frequency interleaved DACs (FI-DACs). The primary application example is a 128 GBd QAM16 coherent optical transceiver. However, the technique is applicable to other types of communication transceivers, and it can be generalized to arbitrary signals, as long as they are stationary or quasi-stationary and have a wideband continuous spectrum. The key elements of the proposed technique are a MIMO equalizer and the *backpropagation* algorithm. Numerical simulation results for the aforementioned application example show that the signal to noise and distortion ratio (SNDR) of the FI-DAC is boosted by more than 25 dB when the proposed compensation technique is applied in the presence of typical analog mismatches. Furthermore, the optical signal to noise ratio penalty of the optical transceiver is reduced from 6 dB to 0.1 dB.

INDEX TERMS Background calibration, error backpropagation, frequency interleaving DAC, high-speed optical transmitter.

I. INTRODUCTION

This paper introduces a novel adaptive background compensation scheme for frequency interleaved digital-to-analog converters (FI-DAC). The primary application example used is a 128 Giga-baud (GBd) 16-quadrature amplitude modulation (QAM16) coherent optical transceiver. However, the technique is applicable to other types of communication transceivers, and it can be generalized to arbitrary signals, as long as they are stationary or quasi-stationary and have a wideband continuous spectrum. Generalization is addressed later in this paper.

Next generation coherent transceivers will operate at symbol rates of $f_B = 1/T = 128 - 150$ GBd and beyond [1]. For a comprehensive review of the state of the art in coherent optical communications, please see [2], [3] and references therein. The main challenge in the design of transceivers for high-speed communications is achieving the large

The associate editor coordinating the review of this manuscript and approving it for publication was Tianhua Xu.

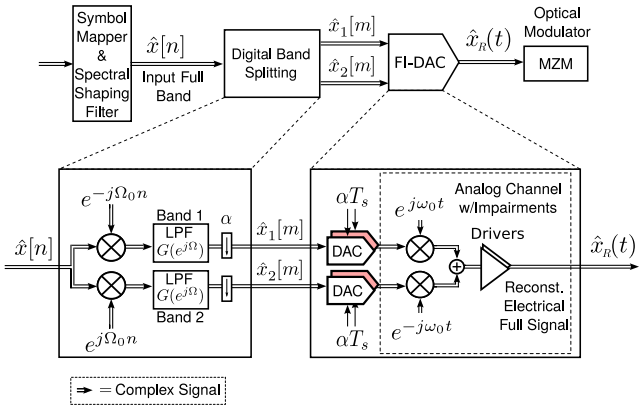

FIGURE 1. Block diagram of a two-band FI-DAC architecture for a DP optical coherent transceiver with $\omega_0 = \frac{2\pi f_B}{4}$, $\Omega_0 = \omega_0 T_s$, and $\alpha = 2$.

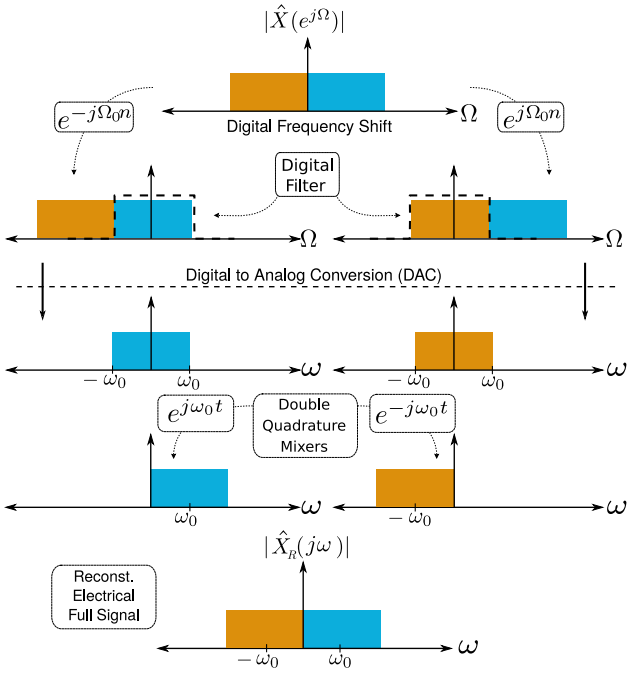

FIGURE 2. Example of the spectra in a two-band FI-DAC architecture.

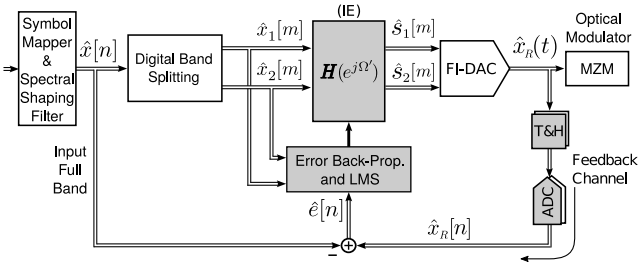

FIGURE 3. Proposed impairment equalizer (IE) with backpropagation adaptation in a two-band FI-DAC based transmitter.

bandwidth (BW) and sampling rate required by the analog-to-digital and the digital-to-analog converters (ADC and DAC). One of the solutions proposed in recent literature is the use of *frequency interleaving* (FI) techniques [4], [5].

Laboratory experiments with high baud rate optical transmission based on FI-DAC have been described in the technical literature [6]. However, significant obstacles remain before this technology can be applied in commercial products. One of the main challenges is how to automatically compensate the impairments of the analog signal path. As a result of process tolerances, layout limitations, etc., errors exist which, if left uncompensated, would introduce large distortions and severely degrade the system performance. Several techniques have been presented to compensate analog errors in FI architectures. In previous work [7] the compensation requires startup calibration, which is done using foreground techniques. In coherent optical systems, the latter would imply the interruption of the communication to compensate the imperfections (particularly when there is a need to track changes over time), which is undesirable. The compensation needs to be accurately tailored to the impairments, which are process, voltage, and temperature dependent and (slowly) time variant. The only way to achieve this at low cost and in a way that lends itself to high volume manufacturing is to use adaptive background compensation techniques. However, no adaptive background compensation techniques for FI-DACs have been reported so far in the technical literature.

The FI-DAC architecture considered in this paper is shown in Fig. 1. It is discussed in the context of its application to a high baud rate transmitter for coherent optical communications. The scheme of Fig. 1 corresponds to one polarization in a dual-polarization (DP) coherent optical transceiver. The transmit path is partitioned into two or more bands by DSP techniques. Without loss of generality, in this paper we assume that it is decomposed into two bands. As shown in Fig. 2, each band is demodulated to baseband with respective complex exponential sequences $e^{\pm j\Omega_0 n}$ where $\Omega_0 = \omega_0 T_s$ with $\omega_0 = (2\pi f_B)/4$ and $1/T_s$ being the DSP sampling rate. The oversampling factor is $N = T/T_s$ with $T = 1/f_B$ being the symbol period. The demodulated baseband signals are first processed by lowpass filters (LPF) with frequency response $G(e^{j\Omega})$, then they are downsampled by a factor α and sinthesized by DACs of lower bandwidth and sampling rate than required by the full signal.[1] After synthesis, analog double quadrature mixers reconstruct the full signal, which, after amplification by a modulator driver, is used to control the Mach-Zehnder Modulator (MZM).[2] The reference clocks of the mixers and the DACs are assumed to be properly synchronized.

Figure 3 depicts a simplified block diagram of the proposed compensation architecture in a two-band FI-DAC based coherent optical transmitter. To compensate the effects of all the analog impairments, we introduce a multiple-input

[1] Typically α is equal to the number of subbands (e.g., $\alpha = 2$ for a two-subband decomposition), although it could be lower and not necessarily an integer.

[2] As discussed in Section II, the analog path compensated by the scheme proposed here includes the impairments of the modulator driver and the interconnections among the FI-DAC, the driver, and the MZM. Said analog path may encompass components in different packages and printed circuit board (PCB) interconnects.

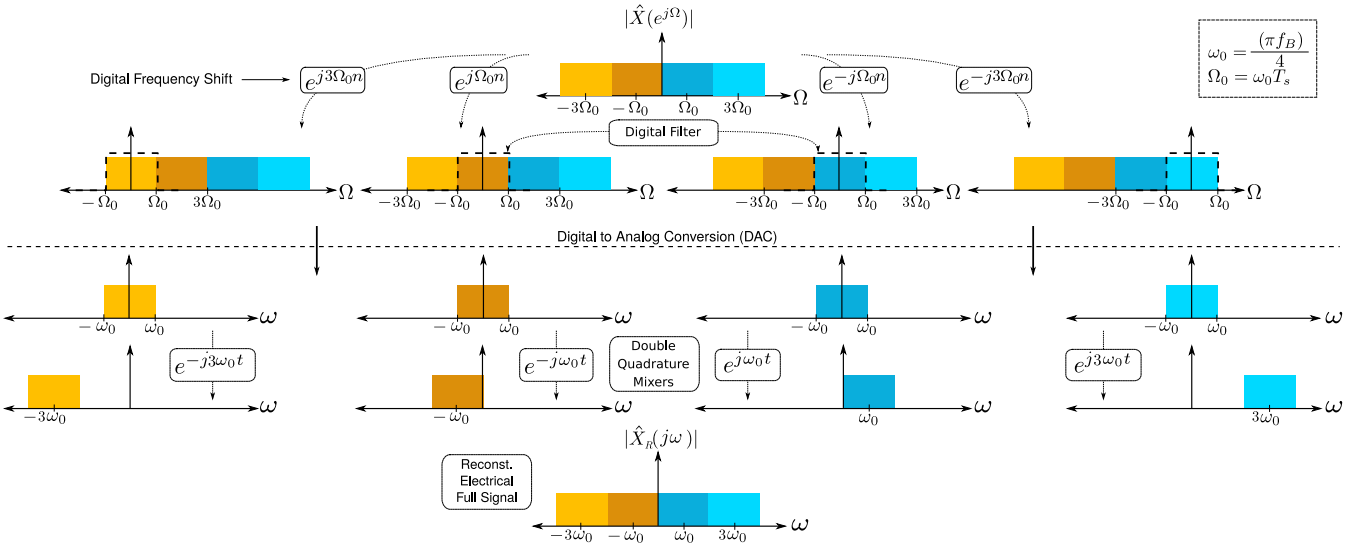

FIGURE 4. Example of the spectra in a four-band FI-DAC architecture.

multiple-output (MIMO) adaptive digital equalizer called hereafter *Impairment Equalizer* (IE), defined by the transfer matrix $\mathbf{H}(e^{j\Omega'})$. Notice that the sampling rate of the signals at the output of the digital band splitting block (i.e., $\hat{x}_1[m]$ and $\hat{x}_2[m]$) is $1/\alpha$ smaller than the sampling frequency of the full input signal. The response of the MIMO IE is adjusted by using the error between the reconstructed analog signal and the original wideband signal. To this end, the reconstructed analog signal $\hat{x}_R(t)$ is sampled by a feedback ADC to get the error signal $\hat{e}[n] = \hat{x}_R[n] - \hat{x}[n]$. This error includes the impact of all the impairments of the analog path up to the input of the MZM. Then, the IE is adapted to minimize the mean squared error (i.e., $E\{|\hat{e}[n]|^2\}$ where $E\{.\}$ is the expectation operator) by using the least mean squares (LMS) algorithm. It is important to observe that, although $\hat{e}[n]$ is the error that must be driven towards zero to achieve the compensation of the analog signal path mismatches, it is not the proper error to adapt the IE since it is not computed directly at the output of the latter. Therefore $\hat{e}[n]$ must be preprocessed before it can be applied to the adaptation of the IE. The digital *backpropagation algorithm* [8], [9] is proposed in this paper to do the required preprocessing and thus enable the background compensation of the channel impairments.[3] As shall be discussed in Section IV, this algorithm provides the *proper* error samples required by the LMS algorithm to adapt the coefficients of the IE. Computer simulations demonstrate that the proposed IE architecture effectively compensates not only the DAC and mixer impairments, but also the amplitude and phase distortions of the electrical paths (e.g., it acts as pre-emphasis and/or precompensator of time skew between in-phase and quadrature (I&Q) components).

In the above discussion, partition into two subbands has been assumed. To process even larger BW signals, this technique can be extended to more subbands, which would require more DACs with similar characteristics as those just described (e.g., see Fig. 4).

The rest of this paper is organized as follows. Section II introduces the channel impairments. Section III presents an overview of the proposed adaptive background compensation technique, while Section IV contains a detailed mathematical formulation. Section V presents simulation results. Sections VI and VII discuss potential generalizations of the technique described here to applications other that digital communications, as well as some limitations of this study and open questions. Finally, conclusions are drawn in Section VIII.

II. ANALOG IMPAIRMENTS IN FI-DAC

Analog impairments drastically affect the performance of any FI-DAC architecture, including the one presented here. The most important ones are the following:

a) **Distortions, bandwidth limitations, and mismatches in the frequency responses of the DACs and the electrical paths between the DACs and the mixers**. Ideally the DACs should have an ideal low pass filter response with a bandwidth equal to one half of the separation between bands, and the signal path from the DACs to the mixers should have infinite bandwidth. In reality, the frequency responses of the DACs are not well controlled: their bandwidths may be larger or smaller than the ideal, and their rolloffs may depart significantly from the ''brick wall'' rolloff of the ideal low pass filter. If the bandwidth is larger and/or the rolloff is softer than ideal, interference between the bands will result. If the bandwidth is less than ideal, a dip in the combined frequency response will result at the boundary between bands.

b) **Time skews at various points in the signal path**. These may result from mismatches in the length of

[3]Alternatively, the *forward propagation algorithm* [10] could be used. This option will be described in detail in a future paper.

the physical paths and/or mismatches in the phase responses of components such as the DACs and the mixers. For example, a mismatch in the phase responses of the DACs corresponding to the two bands will result in an interband time skew. The same effect will result if the physical paths leading from the aforementioned DACs to the mixers have different lengths. Similar effects could arise at the outputs of the mixers and after the summing nodes where the signal is finally reconstructed. One manifestation of these errors of great importance in QAM transmitters is the skew between the in-phase and the quadrature components of the output signal (usually known as I/Q skew).

c) **Amplitude errors of the analog carriers in the reconstruction mixers**. In Fig. 1 the carrier input to the quadrature mixers is represented as a complex exponential $e^{\pm j\omega_0 t}$. But in reality, the real and the imaginary components of this carrier may not have perfectly equal amplitudes. This could result, for example, from mismatches in frequency responses or in the physical lengths of the clock signal paths leading to the quadrature mixers.

d) **Quadrature errors of the analog carriers in the reconstruction mixers**. This effect is related to the previous. The mismatches mentioned in (c) could also cause the (ideally) quadrature carriers in reality not to be exactly at 90° phase. It can be shown that the effect of this error, independently or in combination with the one in (c), is the generation of a complex conjugate carrier, which causes interference in the adjacent band.

e) **Bandwidth limitations and frequency response mismatches of the reconstruction mixers**. These errors impact the overall frequency response of the FI-DAC and could also cause timing skews and interband interference.

f) **Bandwidth limitations and frequency response mismatches in the reconstructed signal paths**. These include the electrical path responses going from the outputs of the quadrature mixers to the optical modulator, as well as the responses of the modulator drivers and any other components in the signal path.

III. OVERVIEW OF THE COMPENSATION TECHNIQUE

In this Section we give an overview of the complete compensation technique without delving into mathematical details. Readers who prefer to focus first on a high-level understanding may read this section and then skip to Section V. A more complete mathematical model is provided in the next section and in the Appendix, which provide enough details for those readers who want to reproduce our results.

Based on simple trigonometric identities and signal processing techniques, we show in the Appendix that the FI-DAC block with impairments can be reformulated as a 4×4 MIMO real channel defined by a 4×4 transfer matrix $\mathbf{F}(j\omega)$ with elements $F_{u,v}(j\omega)$, $u, v \in \{1, \ldots, 4\}$, followed by ideal quadrature modulators (see Fig. 5). Based on this result,

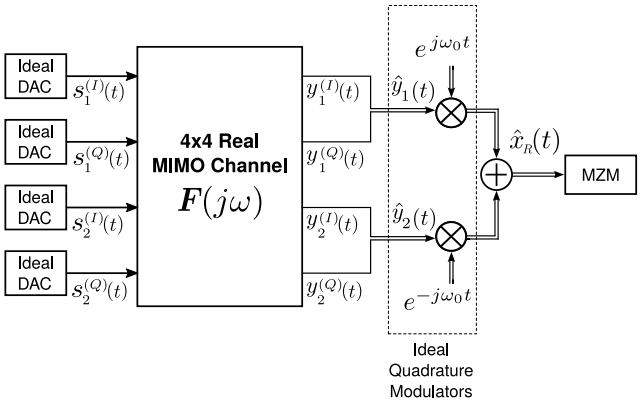

FIGURE 5. Equivalent channel model of analog impairments in a two-band FI-DAC transmitter.

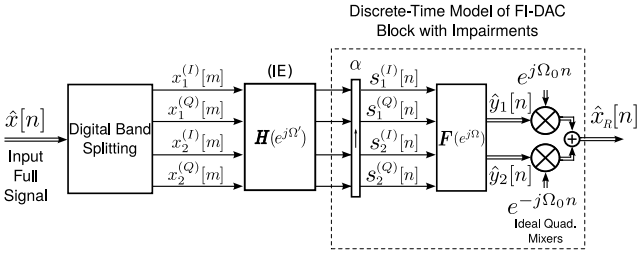

FIGURE 6. Discrete time model of the proposed compensation in a two-band FI-DAC based transmitter.

we can derive a simple discrete time model of the FI-DAC architecture as depicted in Fig. 6. This formulation is important since it shows that all the impairments in FI-DACs can be digitally compensated by a MIMO compensation equalizer (the IE) with transfer matrix $\mathbf{H}(e^{j\Omega'})$. For example, for an ideal compensation, we get $\mathbf{H}_s(e^{j\Omega})\mathbf{F}(e^{j\Omega}) = \mathbf{I}_4$ where $\mathbf{F}(e^{j\Omega})$ is the transfer matrix of the equivalent discrete-time model for the analog impairments sampled at $1/T_s$, $\mathbf{H}_s(e^{j\Omega})$ is the upsampled transfer matrix of the IE, $\mathbf{H}(e^{j\Omega'})$, while $\mathbf{I}_4$ is the 4×4 identity matrix.

The problem that remains to be solved is how to compute $\mathbf{H}_s(e^{j\Omega})$ (or $\mathbf{H}(e^{j\Omega'})$). Since the values of the impairments are not known, and they may vary over time, adaptive feedback techniques are required. The computation is carried out by the IE, which is adapted by the well known LMS algorithm, and the associated blocks (see Fig. 7). Assume for a moment that the output of the block $\mathbf{F}(e^{j\Omega})$, which models the channel impairments, is accessible. Then, the error introduced by the impairments in the output signal could be computed by subtracting the output of the $\mathbf{F}(e^{j\Omega})$ block from the output of the band splitting filters, as is done in the "*Error Computation*" block in Fig. 7. The adaptation algorithm aims to drive this error towards zero. However, this is not the error required by the LMS algorithm, because it is not computed directly from the output of the IE, but from a version of said output filtered by the channel $\mathbf{F}(e^{j\Omega})$. To compensate for the filtering effect of $\mathbf{F}(e^{j\Omega})$, the *backpropagation algorithm* is applied to the output of the "*Error Computation*" block. This is done by the block called "*EBP and Downsamp*"

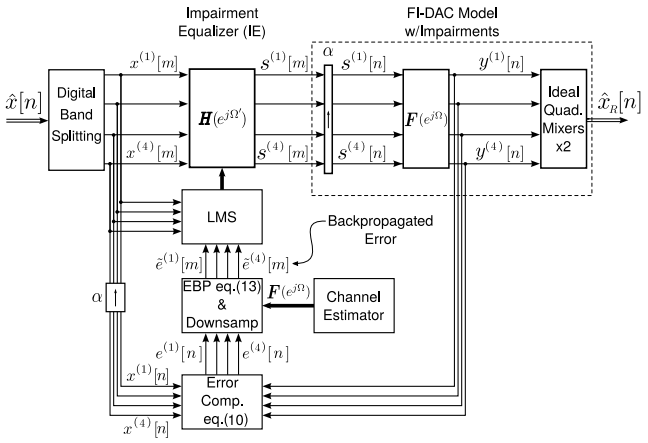

FIGURE 7. Block diagram of the proposed error backpropagation algorithm to estimate the response of the impairment equalizer in a two-band FI-DAC transmitter.

in Fig. 7. The IE can now be adapted by the LMS algorithm, which makes use of the backpropagated error and the output of the "*Digital Band Splitting*" block. However, the "*EBP and Downsamp*" block needs as an input for its computation the coefficients of the channel model $\mathbf{F}(e^{j\Omega})$, which are not directly available. Therefore, a "*Channel Estimator*" (CE) block is introduced (see Fig. 8). This block, whose transfer function is represented as $\hat{\mathbf{F}}(e^{j\Omega})$, is also an adaptive MIMO filter (similar to the IE) adapted by another instantiation of the LMS algorithm (LMS_{CE}).

Since the output of the channel model $\mathbf{F}(e^{j\Omega})$ is not directly available, the output of the entire FI-DAC system including interconnections and possibly buffers, is sampled by an ADC and fed back to the DSP for its use in the IE and CE adaptation. A reduced sampling rate is acceptable for this ADC, since all the adaptation algorithms can be downsampled and run at reduced speed.

IV. ADAPTATION OF THE IMPAIRMENT EQUALIZER (IE): ERROR BACKPROPAGATION ALGORITHM

The samples of the reconstructed full signal can be expressed as (see Figs. 5 and 6):

$$\hat{x}_R[n] = \hat{y}_1[n]e^{j\Omega_0 n} + \hat{y}_2[n]e^{-j\Omega_0 n}, \tag{1}$$

where $\hat{y}_1[n] = y_1^{(I)}[n] + jy_1^{(Q)}[n]$ and $\hat{y}_2[n] = y_2^{(I)}[n] + jy_2^{(Q)}[n]$ with components given by

$$\mathbf{y}[n] = \mathcal{F}^{-1}\{\mathbf{F}(e^{j\Omega})\mathcal{F}\{\mathbf{s}[n]\}\}, \tag{2}$$

where $\mathcal{F}\{.\}$ ($\mathcal{F}^{-1}\{.\}$) denotes the FT (inverse FT) operator, $\mathbf{y}[n]$ is the 4×1 real vector defined by $\mathbf{y}[n] = [y_1^{(I)}[n] \;\; y_1^{(Q)}[n] \;\; y_2^{(I)}[n] \;\; y_2^{(Q)}[n]]^T$ while $\mathbf{s}[n] = [s_1^{(I)}[n] \; s_1^{(Q)}[n] \; s_2^{(I)}[n] \; s_2^{(Q)}[n]]^T$ is the 4×1 real vector with the upsampled digital samples at the inputs of discrete-time model of the channel with impairments given by

$$\mathbf{s}[n] = \mathcal{F}^{-1}\{\mathbf{H}_s(e^{j\Omega})\mathcal{F}\{\mathbf{x}_B[n]\}\}, \tag{3}$$

where $\mathbf{x}_B[n] = [x_1^{(I)}[n] \; x_1^{(Q)}[n] \; x_2^{(I)}[n] \; x_2^{(Q)}[n]]^T$ is the 4×1 real vector with the upsampled outputs of the digital band splitting block (i.e., the sampling frequency is $1/T_s$).[4]

Let $\hat{e}[n]$ be the error signal defined as

$$\hat{e}[n] = \hat{x}_R[n] - \hat{x}[n], \tag{4}$$

where $\hat{x}_R[n]$ is the reconstructed full signal (1), and $\hat{x}[n]$ is the input full signal given by

$$\hat{x}[n] = \hat{x}_1[n]e^{j\Omega_0 n} + \hat{x}_2[n]e^{-j\Omega_0 n} \tag{5}$$

with $\hat{x}_a[n] = x_a^{(I)}[n] + jx_a^{(Q)}[n]$, $a \in \{1, 2\}$, being the upsampled complex signal at the output of the digital band splitting block (see Fig. 7).

The IE response $\mathbf{H}(e^{j\Omega'})$ (or $\mathbf{H}_s(e^{j\Omega})$) is adjusted to minimize of the mean squared error (MSE), $E\{|\hat{e}[n]|^2\}$, by using the LMS algorithm as explained in the following.

A. LMS BASED ADAPTATION OF THE IMPAIRMENT EQUALIZER

Let $H_{u,v}(e^{j\Omega'})$ with $u, v \in \{1, 2, 3, 4\}$ be the (u, v) transfer function of the 4×4 transfer matrix of the IE, $\mathbf{H}(e^{j\Omega'})$. We also define the *real* impulse responses $h_{u,v}[m] = \mathcal{F}^{-1}\{H_{u,v}(e^{j\Omega'})\}$ with $u, v \in \{1, 2, 3, 4\}$. In this work we adopt the LMS (LMS_{IE}) algorithm to iteratively adapt the real coefficients of the set $h_{u,v}[m]$ in order to minimize the MSE, $E\{|\hat{e}[n]|^2\}$, by using

$$\mathbf{h}_{u,v}^{(k+1)} = \mathbf{h}_{u,v}^{(k)} - \beta\nabla_{\mathbf{h}_{u,v}} E\{|\hat{e}[n]|^2\}, \tag{6}$$

where $u, v \in \{1, \ldots, 4\}$, k denotes the number of iteration, $\mathbf{h}_{u,v} = [h_{u,v}[0] \; h_{u,v}[1] \; \cdots \; h_{u,v}[L_h - 1] \;]^T$, L_h is the number of coefficients of the filters, β is the adaptation step, and $\nabla_{\mathbf{h}_{u,v}} E\{|\hat{e}[n]|^2\}$ is the gradient of the MSE with respect to the real vector $\mathbf{h}_{u,v}$.

From (1) and (5), notice that minimizing $E\{|\hat{e}[n]|^2\}$ is equivalent to minimizing the mean of the total squared error of the subband signals,

$$\mathcal{E}[n] = \sum_{a=1}^{2} |\hat{y}_a[n] - \hat{x}_a[n]|^2. \tag{7}$$

Therefore (6) results

$$\mathbf{h}_{u,v}^{(k+1)} = \mathbf{h}_{u,v}^{(k)} - \beta\nabla_{\mathbf{h}_{u,v}} E\{\mathcal{E}[n]\}, \quad u, v \in \{1, \ldots, 4\}, \tag{8}$$

The computation of the gradient of $E\{\mathcal{E}[n]\}$ is not trivial since $\mathcal{E}[n]$ is not the squared of the error at the output of the IE. To get the proper error samples to adapt the coefficients of the filters as expressed in (6), we propose to use the *backpropagation algorithm* widely used in *machine learning* [8], [9].

[4]In this work, time index m is used when the sampling rate is $1/(\alpha T_s)$, while n is used for $1/T_s$ sampling rate.

B. ERROR BACKPROPAGATION (EBP)

For simplicity, we modify the notation of the system model as depicted in Fig. 7. Note that we use an integer index between 1 and 4 to represent a certain component (I or Q) in a given band (1 or 2). Then, the squared error (7) can be rewritten as

$$\mathcal{E}[n] = \sum_{i=1}^{4} |e^{(i)}[n]|^2, \tag{9}$$

where $e^{(i)}[n]$ is the *real* error between the i-th real output of the MIMO channel, $y^{(i)}[n]$, and the i-th upsampled real input of the IE, $x^{(i)}[n]$, i.e., (see Fig. 7)

$$e^{(i)}[n] = y^{(i)}[n] - x^{(i)}[n]. \tag{10}$$

As usual with the stochastic gradient descent (SGD) based adaptation, we replace the gradient of the MSE, $\nabla_{\mathbf{h}_{u,v}} E\{\mathcal{E}[n]\}$, by a noisy estimate, $\nabla_{\mathbf{h}_{u,v}} \mathcal{E}[n]$, i.e.,

$$\mathbf{h}_{u,v}^{(k+1)} = \mathbf{h}_{u,v}^{(k)} - \beta \nabla_{\mathbf{h}_{u,v}} \mathcal{E}[n], \quad u, v \in \{1, \ldots, 4\}. \tag{11}$$

Based on the analysis in the Appendix of [11], it is possible to show that an *instantaneous* gradient of (9) is

$$\nabla_{\mathbf{h}_{u,v}} \mathcal{E}[n] \propto \tilde{e}^{(u)}[m] \overline{\mathbf{x}}^{(v)}[m], \tag{12}$$

where $\overline{\mathbf{x}}^{(v)}[m]$ is the L_h-dimensional real vector with the samples at the input of the IE, i.e.,

$$\overline{\mathbf{x}}^{(v)}[m] = \left[x^{(v)}[m], x^{(v)}[m-1], \cdots, x^{(v)}[m-L_h+1]\right]^T,$$

while $\tilde{e}^{(u)}[m]$ is the *backpropagated error* obtained by downsampling the real error sequence

$$\tilde{e}^{(u)}[n] = \sum_{j=1}^{4} \sum_{l=0}^{L_F-1} f_{j,u}[l] e^{(j)}[n+l], \tag{13}$$

where $f_{u,v}[n]$ is the impulse response of the filter with input u and output v of the MIMO channel $\mathbf{F}(e^{j\Omega})$, while L_F is the number of taps of the filter (see [8]–[10] for a detailed description of the backpropagation technique).

As observed from (13), the knowledge of the MIMO channel response $\mathbf{F}(e^{j\Omega})$ (i.e., $f_{u,v}[n]$) and the subband errors ($e^{(j)}[n]$) is required to evaluate the backpropagated error and the gradient (12). These components can be obtained from the samples of the reconstructed signal $\hat{x}_R(t)$, therefore a feedback channel is required. The feedback path includes buffers and track and holds (T&H) to support the bandwidth of the reconstructed full signal $\hat{x}_R(t)$. The samples are then used by the "*Channel Estimator*" (CE) block to compute the error signals (10) and estimate the MIMO channel response $\mathbf{F}(e^{j\Omega})$, as discussed in the following.

C. CHANNEL ESTIMATOR (CE) BLOCK

The estimation of the analog channel response $\mathbf{F}(e^{j\Omega})$ can be achieved by using the LMS algorithm (LMS_{CE}) and the error between the estimated full band signal ($\hat{x}_E[n]$) and the samples of the reconstructed full signal ($\hat{x}_R[n]$) as depicted in Fig. 8. Notice that CE block is also able to provide samples

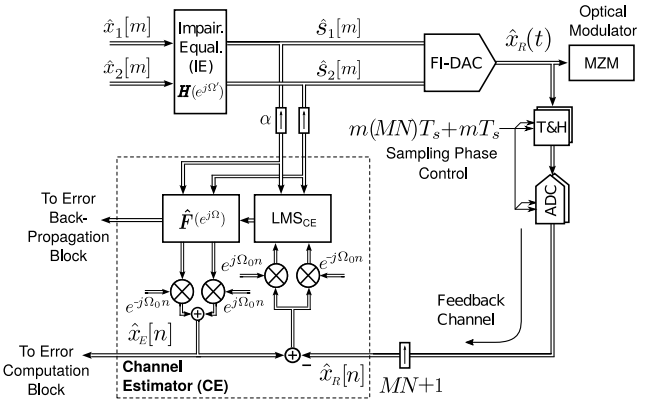

FIGURE 8. Low complexity architecture for estimating the equivalent channel model of analog impairments in a two-band FI-DAC for one polarization in a DP coherent optical transmitter.

of the reconstructed signal at full rate for computation of the error $\hat{e}[n]$. The response of the feedback path (i.e., T&H, ADC) could be initially estimated and removed from $\hat{\mathbf{F}}(e^{j\Omega})$.

Channel impairments change slowly over time, thus the estimation algorithm does not need to operate at full rate. The latter allows implementation complexity to be significantly reduced. For example, low power, low speed (i.e., $1/(MT) = 1/(MNT_s)$ with $M \gg 1$), medium resolution ADCs with adjustable sampling phase can be used. Let t_m be the time instant corresponding to the sample $\hat{x}_R[m]$ (i.e., $\hat{x}_R[m] = \hat{x}_R(t)|_{t=t_m}$). Thus, the m-th time instant of the feedback low speed ADC used to estimate the analog channel is

$$t_m = m(MN)T_s + mT_s. \tag{14}$$

Notice that the sampling period of the feedback channel is $(MN+1)T_s$. Additional complexity reduction is enabled by: 1) strobing the algorithms once they have converged, and/or 2) implementing them in firmware in an embedded processor, typically available in coherent optical transceivers.

V. SIMULATIONS

Using computer simulations, we investigate the performance of the proposed background calibration technique in a two-band FI-DAC-based coherent optical communication system. We assume QAM16 modulation with a symbol rate $f_B = 1/T = 128$ GBd in a back-to-back optical channel. The oversampling factor in the DSP blocks is $N = T/T_s = 1.5$. We assume 8-bit resolution DACs with 96 GS/s sampling rate (i.e., $\alpha = 2$ in Fig. 1) and B_0 =32 GHz nominal BW, which is half of what would be needed to process the input signal band in a non-interleaved architecture. Pulse shaping with raised cosine filters and rolloff factor $\rho = 0.10$ is applied. An ideal feedback channel is assumed. The number of taps of the impairment equalizers is $L_h = 59$. For details of the traditional DSP blocks of a coherent optical transceiver see [2] and references therein.

The impairments of the FI-DAC described in Section II are modeled as follows:

a) *Distortions, bandwidth limitations, and mismatches in the frequency responses of the DACs and the electrical paths between the DACs and the mixers*. We assume four electrical analog path responses, $B_a^{(I/Q)}(j\omega)$ with $a \in \{1, 2\}$ (see Fig. 17), modeled by sixth-order Butterworth lowpass filters with bandwidths $B_0 + \Delta BW_{B_a^{(I/Q)}}$, where B_0 is the nominal bandwidth and $\Delta BW_{B_a^{(I/Q)}}$ is the corresponding bandwidth error.

b) *Time skews*. Although this effect can be introduced at various points in the signal path, we focus on the time delays between $s_a^{(I)}(t)$ and $s_a^{(Q)}(t)$ with $a \in \{1, 2\}$ (i.e., I/Q time skew). These delays, denoted as τ_{s_a}, are generated by four independent Lagrange interpolators (i.e., $\pm\frac{\tau_{s_a}}{2}$ with $a \in \{1, 2\}$).

c) *Amplitude errors of the analog carriers in the reconstruction mixers* and

d) *Quadrature errors of the analog carriers in the reconstruction mixers*. As discussed in the Appendix, the complex carrier in the quadrature mixer a with $a \in \{1, 2\}$ can be written as $p_a(t) = (1 + \delta_a)\cos(\omega_0 t + \phi_a/2) + j(1 - \delta_a)\sin(\omega_0 t - \phi_a/2)$, where δ_a and ϕ_a are the gain and phase errors, respectively. This equation combines the effects of items *c*) and *d*) of this list.

e) *Bandwidth limitations and frequency response mismatches of the reconstruction mixers*. We assume eight electrical analog path responses, $C_{a,b}^{(I/Q)}(j\omega)$ with $a, b \in \{1, 2\}$ (see Fig. 17), modeled by sixth-order Butterworth lowpass filters with bandwidths $2B_0(1 + \rho) + \Delta BW_{C_{a,b}^{(I/Q)}}$, where $2B_0(1+\rho)$ is the nominal bandwidth, $\Delta BW_{C_{a,b}^{(I/Q)}}$ is the corresponding bandwidth error, and ρ is the rolloff factor.

f) *Bandwidth limitations and frequency response mismatches in the reconstructed signal paths*. We assume four electrical analog path responses, $D_a^{(I/Q)}(j\omega)$ with $a \in \{1, 2\}$ (see Fig. 17), modeled by sixth-order Butterworth lowpass filters bandwidths $2B_0(1 + \rho) + \Delta BW_{D_a^{(I/Q)}}$, where $2B_0(1+\rho)$ is the nominal bandwidth and $\Delta BW_{D_a^{(I/Q)}}$ is the corresponding bandwidth error.

A. IMPACT OF THE ANALOG IMPAIRMENTS OF THE FI-DACs

To illustrate the impact on the performance of a coherent optical receiver caused by the different impairments in the transmitter FI-DACs, we show the received constellations in the presence of analog errors for a noise-free optical channel. The parameters used in the simulations are drawn from uniform distributions in the intervals detailed in Table 1. Please notice that there is a one to one correspondence of the items of the list given above with the scenarios of rows *a*) through *f*) of Table 1, as well as with the list of Section II describing the impairments. The simulations of Fig. 9 use parameters from one particular sample from the distributions. For example, the eight values of relative bandwidth errors of $C_{a,b}^{(I/Q)}(j\omega)$ are eight random numbers drawn from a uniform distribution in the interval $[-12.5\%, 25.4\%]$. Although for simplicity the specific numerical values used in our simulation are not shown, the simulation results of Fig. 9 are typical and different random samples produce very similar results. Figures 9 *(a)* through *(f)* show results with the proposed compensation off and mismatches exercised one at a time according to their type (i.e., BW errors, phase errors, I/Q time skew τ_{s_a}, etc.), while Fig. 9-*g* depicts the case with all the impairments simultaneously active (see Table 1 and Fig. 17 for a detailed description of the simulated scenarios). From these figures notice that the analog mismatches severely degrade the transmitted signal. The worst case occurs when all random errors are applied simultaneously. The great improvement enabled by the proposed compensation scheme can be seen in the constellation of Fig. 9-*h*.

TABLE 1. Description of the cases analyzed in Fig. 9. Note that $a, b \in \{1, 2\}$ (see Fig.17). Errors are generated randomly according to a uniform distribution.

Scenario	Effect	Mismatch Range	IE
a)	$B_a^{(I/Q)}(j\omega)$	$\Delta BW \in [-13\%, +17.8\%]$	Disabled
b)	τ_{s_a}	$[-1.8\text{ps}, +1.9\text{ps}]$	Disabled
c)	δ_a	$[0, 0.6]$	Disabled
d)	ϕ_a	$[-30.3^o, +51.7^o]$	Disabled
e)	$C_{a,b}^{(I/Q)}(j\omega)$	$\Delta BW \in [-12.5\%, +25.4\%]$	Disabled
f)	$D_a^{(I/Q)}(j\omega)$	$\Delta BW \in [-18.7\%, +23.3\%]$	Disabled
g)	all	same as scenarios a) to f)	Disabled
h)	all	same as scenarios a) to f)	Enabled

B. PERFORMANCE OF THE IMPAIRMENT EQUALIZER

We focus on the optical signal-to-noise ratio (OSNR) penalty[5] at a bit-error-rate (BER) of 10^{-3}, which is computed using an ideal software receiver. Figure 10 shows the OSNR penalty as a function of the bandwidth mismatches, the gain and phase errors of the quadrature mixers, and the I/Q time skew error. Only one effect is exercised in each case. To stress the mismatch effects, the impairments are introduced as follows: a) BW errors in the responses $B_1^{(I)}(j\omega)$ and $B_2^{(Q)}(j\omega)$ with $\Delta BW_{B_1^{(I)}} = \Delta BW_{B_2^{(Q)}}$, b) I/Q time skew at the outputs of the DACs with $\tau_{s_1} = \tau_{s_2}$, c) BW errors in the responses $C_{1,1}^{(I)}(j\omega)$ and $C_{2,1}^{(Q)}(j\omega)$ with $\Delta BW_{C_{1,1}^{(I)}} = \Delta BW_{C_{2,1}^{(Q)}}$, d) BW errors in the responses $D_1^{(I)}(j\omega)$ and $D_2^{(Q)}(j\omega)$ with $\Delta BW_{D_1^{(I)}} = \Delta BW_{D_2^{(Q)}}$, e) phase ($\phi_a$) and f) gain ($\delta_a$) errors of the two quadrature mixers with $\phi_1 = \phi_2$ and $\delta_1 = \delta_2$. The affected parameters are swept together. We present results with and without the proposed background compensation technique. The effectiveness of the IE architecture is verified in all cases. Notice that the proposed FI-DAC scheme performance is excellent even in the presence of BW errors.

C. MONTECARLO SIMULATIONS

The robustness of the proposed compensation scheme was assessed by Montecarlo simulations. A total of 500 channels with uniformly distributed random impairments such as gain

[5] See [12] for a definition of OSNR penalty.

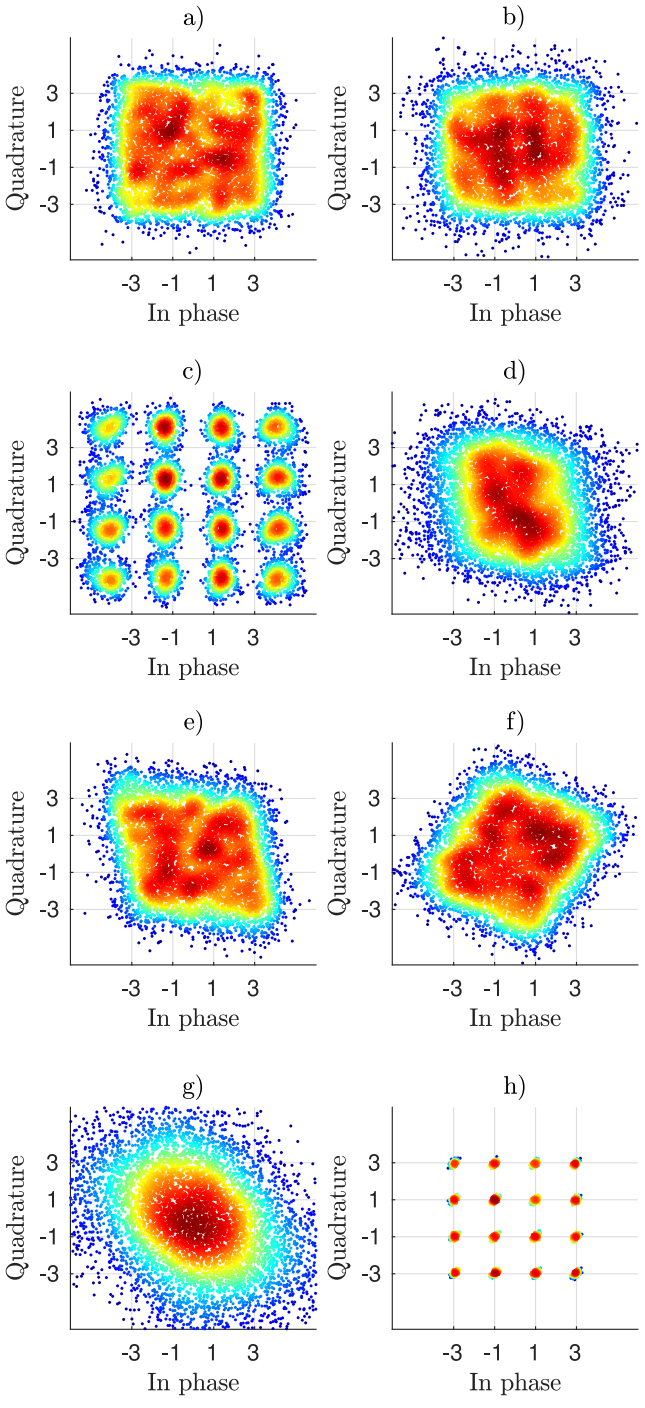

FIGURE 9. Received QAM16 constellation in the presence of analog mismatches with a two-band FI-DACs transmitter. For a detailed description of the test scenarios see Table 1.

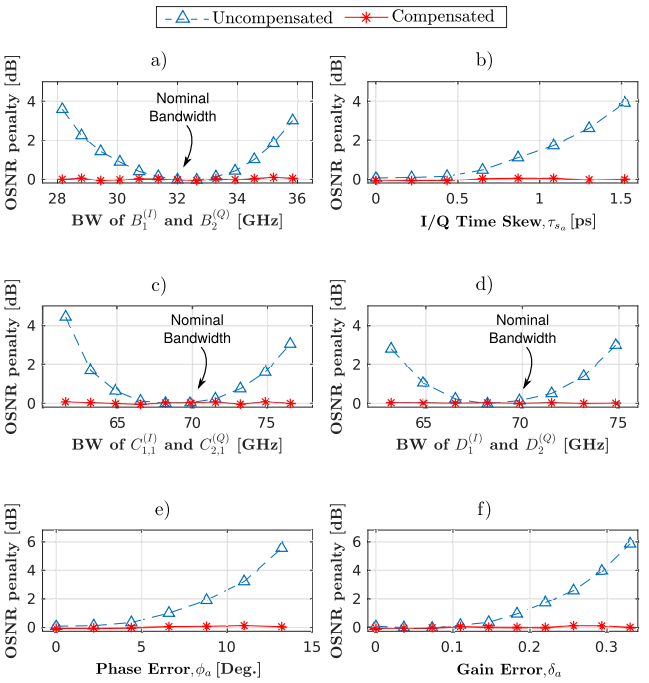

FIGURE 10. OSNR penalty comparison at BER = 10^{-3} versus analog mismatches in a two-band FI-DAC-based transmitter.

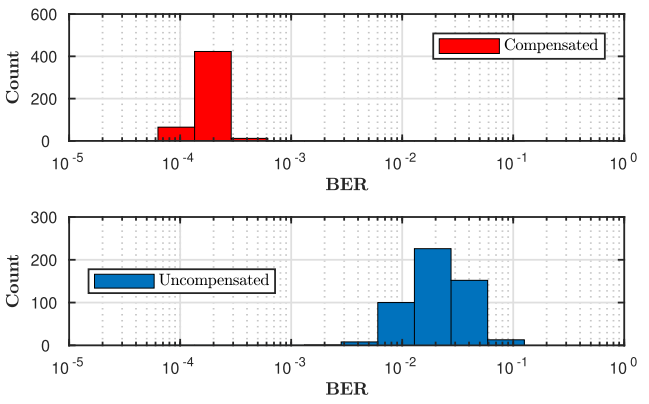

FIGURE 11. Histogram of BER for 500 random analog channels with and without compensation for a BER reference of $\sim 2 \times 10^{-4}$.

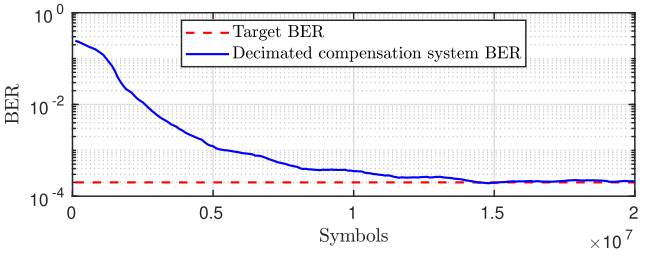

FIGURE 12. BER evolution during convergence of the proposed IE with subsampling of the feedback ADC ($M = 128$). The BER reference in the absence of analog impairments is $\sim 2 \times 10^{-4}$.

errors ($\delta_a \in [\pm 0.25]$), phase errors ($\phi_a \in [\pm 18°]$), I/Q time skew ($\tau_{s_a} \in \pm 25\%$, and bandwidth errors ($\Delta BW_{\mathcal{X}}/B_{\mathcal{X}} \in [\pm 25\%]$ where $B_{\mathcal{X}}$ is the corresponding nominal BW and $\mathcal{X} \in [B_a^{(I/Q)}(j\omega), C_{a,b}^{(I/Q)}(j\omega), D_a^{(I/Q)}(j\omega)]$), were simulated. We set the OSNR to that required to achieve a BER $\sim 2 \times 10^{-4}$ in the absence of analog impairments. Figure 11 shows the histogram of the BER for the system with and without the MIMO equalizer. In all cases the excellent compensation of the impairments achieved by the proposed IE architecture is verified.

Figure 12 depicts one example of the BER evolution in the presence of analog impairments using subsampling of the

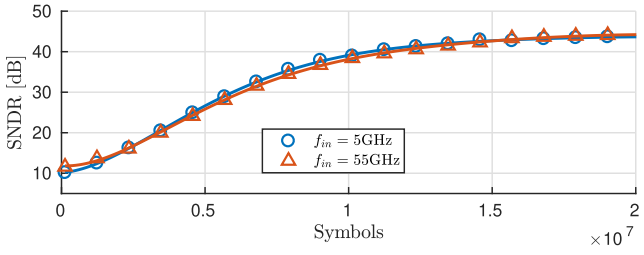

FIGURE 13. SNDR evolution during convergence of the proposed IE with subsampling of the feedback ADC ($M = 128$) for sinusoidal inputs with frequencies f_{in} =5GHz and 55GHz. The SNDR reference in the absence of analog impairments is ∼ 44dB.

feedback ADC with $M = 128$. The target BER without analog errors is $\sim 2\times10^{-4}$. The results confirm the effectiveness of the compensation system in the presence of decimation.

D. SNDR OF THE FI-DAC WITH THE PROPOSED IE

The signal-to-noise-and-distortion ratio (SNDR) is usually used to measure the quality of the signal generated by a DAC. To evaluate the SNDR of the FI-DAC with the proposed impairment equalizer, the spectrum of the reconstructed analog signal $\hat{x}(t)$ is analyzed using a digital real tone as input signal, i.e., $x[n] = \cos(2\pi f_{in} T_s)$. Figure 13 shows the evolution of the SNDR achieved by the system for a subsampled feedback ADC with $M = 128$. We consider the same set of analog errors used in Fig. 12. To obtain the SNDR values, the coefficients of the IE employed to calculate the BER in Fig. 12 (which are evolving all along as the background compensation system performs the adaptation), are saved at certain points of the convergence evolution. Then, those coefficients are loaded to the system, and the SNDR of the output signal is measured. The same approach is used to evaluate two input frequencies: $f_{in} = 5$GHz and 55GHz. The target SNDR is ∼ 44dB. The results confirm the effectiveness of the compensation system in the presence of decimation. The spectra of the output signals for a sinusoidal tone at the input at the beginning (uncompensated) and at the end (compensated) of convergence are shown in Fig. 14. In the uncompensated case, the presence of spurs degrades the SNDR of the whole system. At the end of the convergence in the compensated scheme, complete mitigation of the spurs is accomplished. The SNDR curves for a frequency sweep at the input are depicted in Fig. 15. The same set of analog errors used in Fig. 14 is considered. Note that the SNDR degradation in the presence of all errors exercised at the same time and without compensation is more than 25dB for all frequencies.

VI. GENERALIZATION TO OTHER APPLICATIONS

The scope of this paper has been deliberately limited to the example of the transmitter in a coherent optical transceiver. However the technique presented here can be generalized to other applications not related to digital communications. The only condition necessary for the technique to be applicable is that the input to the FI-DAC be a stationary or quasi-stationary signal and that its spectrum

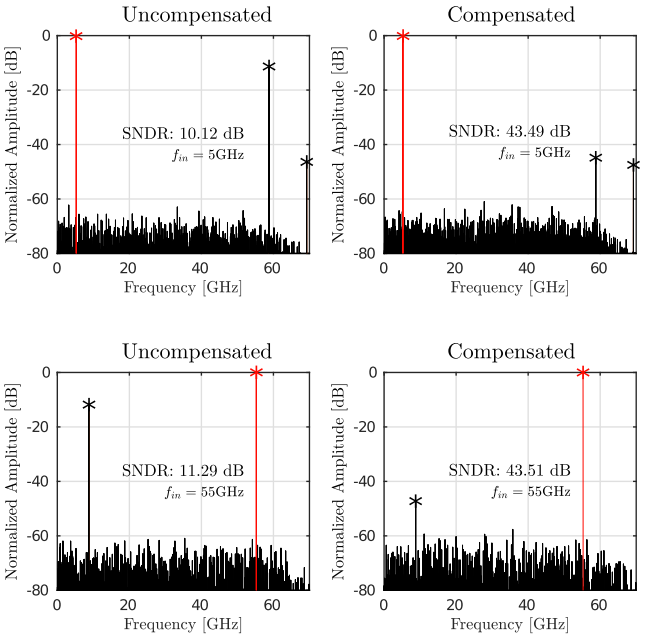

FIGURE 14. Frequency domain spectra of the output signals, for a sinusoidal tone at the input (f_{in} = 5GHz tone and f_{in} = 55GHz tone), uncompensated (left) and compensated (right) in a decimated compensation system, see Fig13.

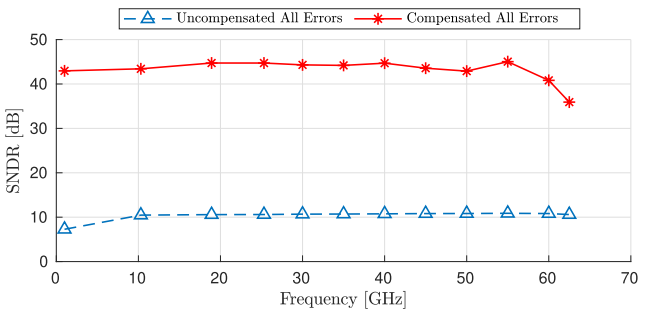

FIGURE 15. SNDR performance for a frequency sweep at the input. Mismatch errors applied in the simulation for all impairments are in intervals of ±10% of their ideal values.

be wideband and continuous. The stationarity or quasi-stationarity condition is necessary because the adaptation of the IE and the CE is relatively slow and it can only track signals whose properties change slowly in time. The wide spectrum condition is required to ensure that the IE and the CE have feedback at all frequencies within their band of operation, so that convergence and stability can be guaranteed. However, even in applications where the stationarity and wide spectrum conditions cannot be met, it is possible to use this technique in foreground mode. In this case the IE and the CE are trained during an initialization period using a synthetic signal which meets the above conditions, for example a pseudo-random binary sequence (PRBS), and then both adaptive filters are frozen and normal operation of the FI-DAC starts. At this point the FI-DAC system is ready to be used with arbitrary signals, including narrowband and non-stationary signals. This is essentially what was done in the simulation study of Section V-D.

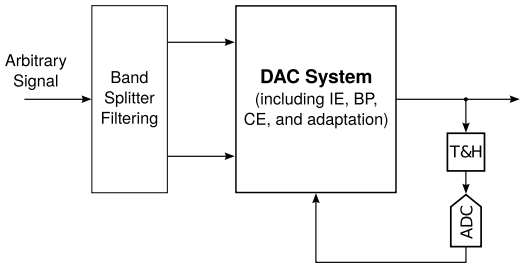

FIGURE 16. Generalization to other applications.

The practical application would mimic the procedure of the simulation.

Figure 16 shows how the DAC system is used in a generic application. Examples of applications not related to communications are radar [13], arbitrary waveform generators (AWG) [14], test and measurement equipment [15], and instrumentation for physics research. Additionally, even in digital communications, the technique can be extended to applications that the present work did not cover. For example, it can be used to precompensate the transmitter in wireline or wireless applications, as well as in intensity modulation and direct detection (IM/DD) channels.

VII. LIMITATIONS OF THE STUDY AND FUTURE WORK

The present work addressed the FI-DAC topology, but similar techniques can be applied to alternative topologies such as time interleaving and analog multiplexing DACs. Furthermore, the proposed technique was analyzed at a high level and in a conceptual way, but future work will address the implementation level. A large body of work is currently underway to develop proofs of concept in laboratory experiments and in integrated circuits. An experimental platform is being developed, which is expected to motivate new research on compensation techniques for ultra high performance data converters.

VIII. CONCLUSION

A FI-DAC architecture with adaptive background compensation of the analog signal path errors has been presented. Simulations confirm the effectiveness of the proposed technique, which shows more than 25 dB of SNDR improvement in a frequency sweep in the band of interest. This results in the essentially complete elimination of the penalty caused by the DAC frequency response and the gain and phase errors in the mixers, as well as other impairments. Although the technique was presented in the context of a transmitter for coherent optical communications, it is more general and suitable not only in other communication applications such as IM-DD but also in the presence of arbitrary wideband signals.

APPENDIX

In this Appendix we derive the channel model of Fig. 5. Figure 17 shows a block diagram of a two-band FI-ADC with all the impairments as described in Sections II and V. With a proper design, it is possible to assume that the *two cosine (and*

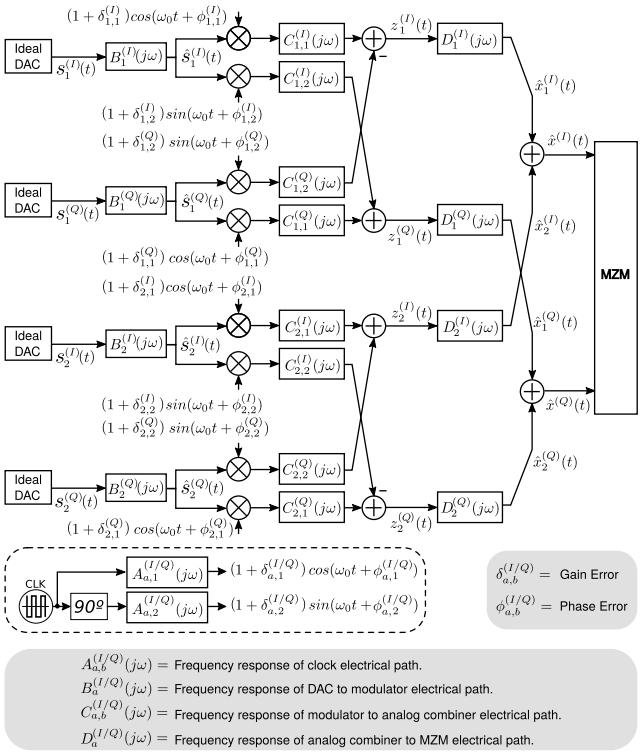

FIGURE 17. Model of analog impairments in a two-band FI-DAC based transmitter.

sine) signals used in each quadrature mixer have the same gain and phase,[6] i.e., $\delta_{a,1}^{(I)} = \delta_{a,1}^{(Q)} = \delta_a$; $\delta_{a,2}^{(I)} = \delta_{a,2}^{(Q)} = -\delta_a$; $\phi_{a,1}^{(I)} = \phi_{a,1}^{(Q)} = \phi_a/2$, and $\phi_{a,2}^{(I)} = \phi_{a,2}^{(Q)} = -\phi_a/2$ with $a \in \{1, 2\}$. Note that δ_a and ϕ_a represent the gain and phase imbalance of the quadrature mixer for band a, respectively. On the other hand, the mismatches between the responses of the electrical paths that arrive at each adder of the quadrature modulator can be assumed small (e.g., $C_{a,1}^{(I)}(j\omega) \approx C_{a,2}^{(Q)}(j\omega)$ and $C_{a,2}^{(I)}(j\omega) \approx C_{a,1}^{(Q)}(j\omega)$ with $a \in \{1, 2\}$). Therefore, the responses $C_{a,b}^{(I/Q)}(j\omega)$ can be moved after the adders and included in the corresponding filters $D_a^{(I/Q)}(j\omega)$, as shown in Fig. 18. The good accuracy of this assumption is verified through simulations in Section V.

Then, based on the complex model proposed in [16], the modulator output of band a denoted as $z_a(t) = z_a^{(I)}(t) + jz_a^{(Q)}(t)$ (see Fig. 17), can be expressed as

$$z_a(t) = \hat{s}_a(t)p_a(t), \quad a \in \{1, 2\}, \tag{15}$$

where $\hat{s}_a(t) = \hat{s}_a^{(I)}(t) + j\hat{s}_a^{(Q)}(t)$ is the mixer input, and

$$p_a(t) = k_{a,1}e^{j\omega_0 t} + k_{a,2}e^{-j\omega_0 t} \tag{16}$$

with complex constants given by

$$k_{1,1} = k_{1,1}^{(I)} + jk_{1,1}^{(Q)} = \frac{1+\delta_1}{2}e^{j\phi_1/2} + \frac{1-\delta_1}{2}e^{-j\phi_1/2}, \tag{17}$$

[6] Although this assumption simplifies the math, it can be shown that it is not necessary for the applicability of the compensation scheme proposed in this paper.

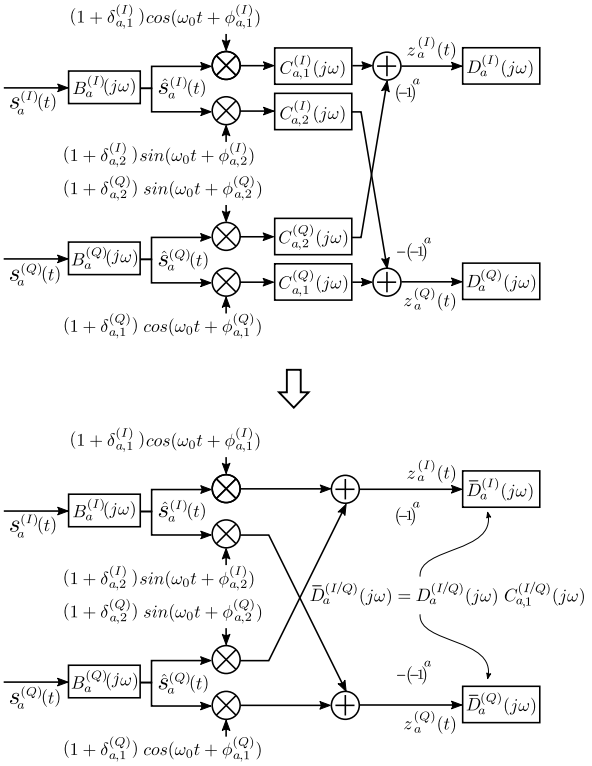

FIGURE 18. Simplification of the responses $C_{a,b}^{(I/Q)}(j\omega)$ for an equivalent complex channel model approach.

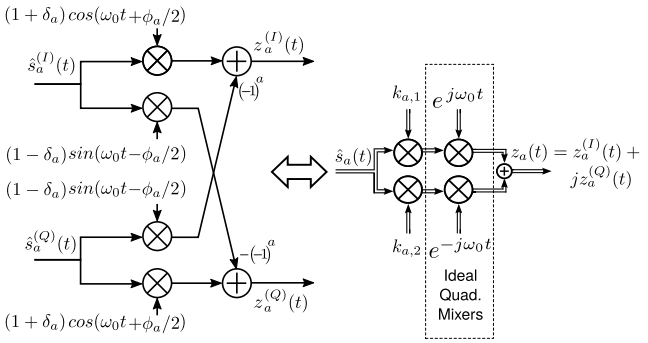

FIGURE 19. Equivalent complex channel model of a quadrature mixer with I/Q imbalance for the subband $a \in \{1, 2\}$.

$$k_{1,2} = k_{1,2}^{(I)} + jk_{1,2}^{(Q)} = \frac{1+\delta_1}{2}e^{-j\phi_1/2} - \frac{1-\delta_1}{2}e^{j\phi_1/2}, \quad (18)$$

$$k_{2,1} = k_{2,1}^{(I)} + jk_{2,1}^{(Q)} = \frac{1+\delta_2}{2}e^{j\phi_2/2} - \frac{1-\delta_2}{2}e^{-j\phi_2/2}, \quad (19)$$

$$k_{2,2} = k_{2,2}^{(I)} + jk_{2,2}^{(Q)} = \frac{1+\delta_2}{2}e^{-j\phi_2/2} + \frac{1-\delta_2}{2}e^{j\phi_2/2}. \quad (20)$$

In the absence of gain and phase errors, notice that $p_1(t) = e^{j\omega_0 t}$ and $p_2(t) = e^{-j\omega_0 t}$. Figure 19 shows the equivalent complex-valued model of the quadrature mixer with impairments. The quadrature mixer outputs $z_a^{(I/Q)}(t)$ are transmitted up to the optical modulator through electrical paths (which include the modulator drivers) with mismatch responses $\overline{D}_a^{(I/Q)}(j\omega)$ (see Fig. 17). From (15) and Fig. 20, the complex

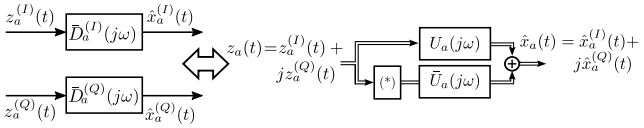

FIGURE 20. Complex-valued channel model of the mixer-MZM electrical paths with responses $\overline{D}_a^{(I/Q)}(j\omega)$ for the subband $a \in \{1, 2\}$ (see Fig. 17).

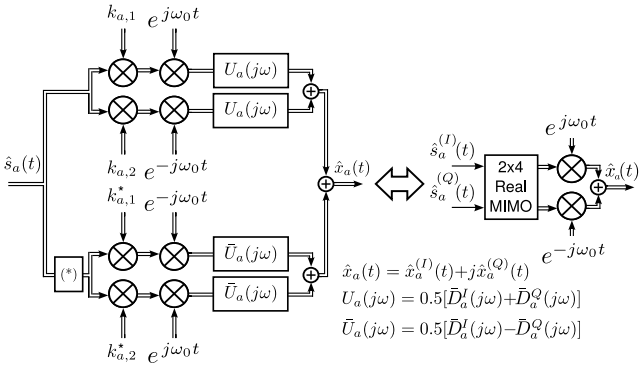

FIGURE 21. Equivalent MIMO channel model of the combined quadrature mixer and mixer-MZM electrical paths for the subband $a \in \{1, 2\}$.

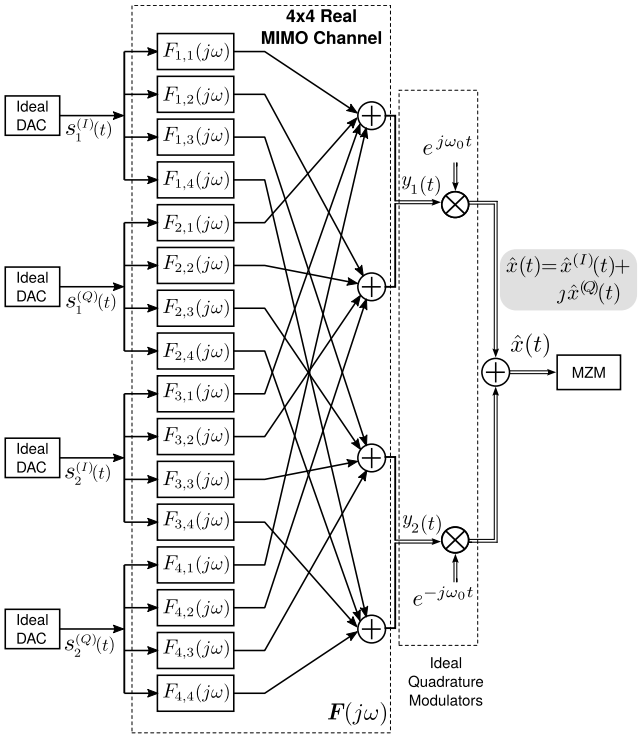

FIGURE 22. Equivalent channel model of analog impairments in a two-band FI-DAC for one polarization in a DP coherent optical transmitter.

signal at the MZM input can be expressed as

$$\hat{x}_a(t) = z_a^{(I)}(t) \otimes \overline{d}_a^{(I)}(t) + jz_a^{(Q)}(t) \otimes \overline{d}_a^{(Q)}(t), \quad (21)$$

where symbol $\otimes$ denotes the convolution operation and $\overline{d}_a^{(I/Q)}(t) = \mathcal{F}^{-1}\{\overline{D}_a^{(I/Q)}(j\omega)\}$. Since $z_a^{(I)}(t) = 0.5[z_a(t) + z_a^*(t)]$ and $jz_a^{(Q)}(t) = 0.5[z_a(t) - z_a^*(t)]$, we can get

$$\hat{x}_a(t) = z_a(t) \otimes u_a(t) + z_a^*(t) \otimes \overline{u}_a(t), \quad (22)$$

where $u_a(t) = 0.5[\overline{d}_a^{(I)}(t) + \overline{d}_a^{(Q)}(t)]$ and $\overline{u}_a(t) = 0.5[\overline{d}_a^{(I)}(t) - \overline{d}_a^{(Q)}(t)]$ (see Fig. (20)).

From the above, we can derive the channel model for the quadrature mixer with impairments including the electrical paths as shown in the block diagram on the left side of Fig. 21. Moreover, taking into account that $\hat{s}_a(t)e^{\pm j\omega_0 t} \otimes u(t) = [\hat{s}_a(t) \otimes u(t)e^{\mp j\omega_0 t}]e^{\pm j\omega_0 t}$, it is possible to exchange the order of the modulator and filter blocks $u_a(t)$ and $\overline{u}_a(t)$. Then, grouping the signals properly, the analog channel for the subband a can be reduced to a 2×4 MIMO real channel followed by two ideal quadrature mixers as depicted on the right side of Fig. 21. Notice that the response of the DAC-mixer electrical paths (i.e., $B_a^{(I/Q)}(j\omega)$ in Fig. 17) can be easily included within this MIMO channel model. Finally, the model just described is applied to the two subbands which are combined resulting in the 4×4 MIMO real channel model of Fig. 22 (and Fig. 5).

REFERENCES

[1] M. Nakamura, F. Hamaoka, A. Matsushita, H. Yamazaki, M. Nagatani, T. Kobayashi, Y. Kisaka, and Y. Miyamoto, "Advanced DSP technologies with symbol-rate over 100-gbaud for high-capacity optical transport network," in *Proc. Opt. Fiber Commun. Conf.*, 2018, pp. 1–3.

[2] D. A. Morero, M. A. Castrillon, A. Aguirre, M. R. Hueda, and O. E. Agazzi, "Design tradeoffs and challenges in practical coherent optical transceiver implementations," *J. Lightw. Technol.*, vol. 34, no. 1, pp. 121–136, Jan. 1, 2016.

[3] M. S. Faruk and S. J. Savory, "Digital signal processing for coherent transceivers employing multilevel formats," *J. Lightw. Technol.*, vol. 35, no. 5, pp. 1125–1141, Mar. 1, 2017.

[4] P. J. Pupalaikis, B. Yamrone, R. Delbue, A. S. Khanna, K. Doshi, B. Bhat, and A. Sureka, "Technologies for very high bandwidth real-time oscilloscopes," in *Proc. IEEE Bipolar/BiCMOS Circuits Technol. Meeting (BCTM)*, Sep. 2014, pp. 128–135.

[5] M. Nakamura, F. Hamaoka, M. Nagatani, H. Yamazaki, T. Kobayashi, A. Matsushita, S. Okamoto, H. Wakita, H. Nosaka, and Y. Miyamoto, "104 Tbps/carrier probabilistically shaped PDM-64QAM WDM transmission over 240 km based on electrical spectrum synthesis," in *Proc. Opt. Fiber Commun. Conf. (OFC)*, 2019, pp. 1–3.

[6] X. Chen, S. Chandrasekhar, G. Raybon, S. Olsson, J. Cho, A. Adamiecki, and P. Winzer, "Generation and intradyne detection of single-wavelength 1.61-Tb/s using an all-electronic digital band interleaved transmitter," in *Proc. Opt. Fiber Commun. Conf. Postdeadline Papers*, Mar. 2018, pp. 1–3.

[7] C. Schmidt, *Interleaving Concepts for Digital-to-Analog Converters Algorithms, Models, Simulations and Experiments*. Wiesbaden, Germany: Springer, 2020.

[8] D. E. Rumelhart, G. E. Hinton, and R. J. Williams, "Learning representations by back-propagating errors," *Nature*, vol. 323, no. 6088, pp. 533–536, Oct. 1986.

[9] I. Goodfellow, Y. Bengio, and A. Courville, *Deep Learning*. Cambridge, MA, USA: MIT Press, 2016.

[10] D. A. Morero, M. R. Hueda, and O. E. Agazzi, "Forward and backward propagation methods and structures for coherent optical receiver," U.S. Patent 10 128 958, Nov. 13, 2018.

[11] F. Solis, B. T. Reyes, D. A. Morero, and M. R. Hueda, "On the application of error backpropagation to the background calibration of time interleaved ADC for digital communication receivers," 2020, *arXiv:2008.02914*. [Online]. Available: http://arxiv.org/abs/2008.02914

[12] C. C. K. Chan, *Optical Performance Monitoring: Advanced Techniques for Next-Generation Photonic Networks*. New York, NY, USA: Academic, Feb. 2010.

[13] H. Deng, *Radar Networks*. Boca Raton, FL, USA: CRC Press, 2020. [Online]. Available: https://books.google.com.ar/books?id=ovDqDwAAQBAJ

[14] (2020). *AWG70000B Series Arbitrary Waveform Generators, Tektronix, 2020, v4*. [Online]. Available: https://download.tek.com/datasheet/AWG70000BDatasheetDraft-19Oct2020-v4.pdf

[15] (2014). *3-Bit DAC Application Note*. SHF Communication Technologies AG, 2014, v001. [Online]. Available: https://www.shf-communication.com/wp-content/uploads/appnotes/shf_app_note_611_c.pdf

[16] E. P. da Silva and D. Zibar, "Widely linear equalization for IQ imbalance and skew compensation in optical coherent receivers," *J. Lightw. Technol.*, vol. 34, no. 15, pp. 3577–3586, Aug. 1, 2016.

AGUSTÍN C. GALETTO (Graduate Student Member, IEEE) was born in Córdoba, Argentina, in 1992. He received the Electronic Engineering degree from the Universidad Tecnológica Nacional Facultad Regional Córdoba (UTN FRC), in 2017. He is currently pursuing the Ph.D. degree with the Microelectronics and Mixed-Signal Design Group, Fundación Fulgor. His Ph.D. research focuses on high-speed coherent transmitters. Since March 2016, he has been carrying out research and development activities with the Microelectronics and Mixed-Signal Design Group, Fundación Fulgor. His research interests include mixed signal circuits, such as DAC and its calibration and compensation systems, embedded systems applications, and new integration technologies applied to electronics and telecommunications.

BENJAMÍN T. REYES was born in Río Tercero, Argentina, in 1982. He received the degree in electronic engineering from the Universidad Tecnológica Nacional, Córdoba, Argentina, in 2008, and the Ph.D. degree in engineering form the Universidad Nacional del Sur, Bahía Blanca, Argentina, in 2015. He is currently a member of the Research Staff with Fundación Fulgor and the Senior Analog Designer with Inphi Argentina. His current research interests include high-speed analog-to-digital converters, high-speed mixed-signal circuits design, and digital-assisted analog design for digital communications applications.

DAMIÁN A. MORERO was born in Córdoba, Argentina. He received the degree (Hons.) in electronic engineering and the Ph.D. degree in engineering science from the National University of Córdoba (UNC), Córdoba. He is currently the Senior Director Research and Development with Inphi Argentina, where he has been engaged in the research and development of error correction coding schemes and digital signal processing algorithms for high speed optical communications. His research interests include coding, information theory, signal processing, computer science, and VLSI design. He received the Academic Excellence Award from the Engineers Association, Córdoba, and the UNC, in 2003 and 2005, respectively. From 2006 to 2009, he received Ph.D. fellowships from the Secretary of Science and Technology (SeCyT), Argentina.

MARIO R. HUEDA was born in Jujuy, Argentina. He received the Electrical and Electronic Engineer degree and the Ph.D. degree from the National University of Córdoba, Argentina, in 1994 and 2002, respectively. Since 1994, he has been with the Digital Communications Research Laboratory, Department of Electronic Engineering, National University of Córdoba. He is also with National Scientific and Technological Research Council of Argentina (CONICET). He has 50 patents issued or pending, and has published more than 70 technical papers in journals and conferences. His research interests include digital communications, signal processing, and synchronization.